ACS APPLIED NANO MATERIALS

www.acsanm.org Article

Ag Nanoparticle-Coated Polystyrene Microspheres for Electromagnetic Interference Shielding Films with Low Metal Content

Hua Cheng, Siqi Liu, Ruiqi Wang, Wei Zhang, Rui Pan, Zhe Li, Yi Gong,* Fangkuo Wang, Rui Hu, Jianjun Ding, Xian Zhang, Chen Lin, Jianying He, and Xingyou Tian*

Cite This: ACS Appl. Nano Mater. 2022, 5, 5292−5301 Read Online

ACCESS | Metrics & More | Article Recommendations | Supporting Information

ABSTRACT: The fabrication of thin composite films incorporating metal-based fillers with a delicate structure to achieve high electromagnetic interference shielding effectiveness (EMI SE) at low metal content remains a great challenge. In this work, benefiting from the excellent electrical conductivity of Ag nanoparticles, Ag nanoparticle-coated polystyrene (PS@Ag) microspheres with a large PS core were selected as electrically conductive fillers, and the volume exclusion effect guaranteed the construction of an electrically conductive network with low silver loading. A spontaneous process to construct a segregated laminar structure with a three-dimensional electrically conductive network happened with the assistance of a gravity-driven effect. The flexible thin films with a low amount of silver exhibited outstanding EMI SE per unit thickness (SE/d). To further investigate the effect of the structure on the EMI SE efficiency, it is found that the alternate interfaces play a critical role in enhancing shielding performance by stacking multiple films compared to the bulk films obtained by casting. The EMI SE for an only 0.3 mm triple-piece stacking film with 6.3 wt % Ag loading could reach 55.3 dB compared to 37.2 dB for the triple-thickness casting film. Using the stacking process results in easy accessibility for tailored composites with the desired EMI SE, which supplies a new strategy for the design of shielding materials in the next-generation electronics.

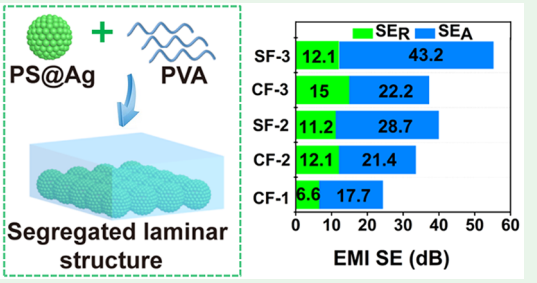

KEYWORDS: *electromagnetic interference, shielding effectiveness, microspheres, alternate interfaces, stacking film*

INTRODUCTION

With electronic instruments evolving toward high integration, light weight, and high frequency, electromagnetic interference (EMI) caused by electromagnetic wave radiation has attracted intensive attention. EMI not only is harmful to the human health but also affects nearby electronic components. Furthermore, the leakage of electromagnetic signals threatens information security.[1] Therefore, research on high EMI shielding effectiveness (SE) materials has become an urgent need to meet the increasing requirements for electromagnetic radiation protection. Until now, polymer-based electromagnetic shielding composite materials have been extensively developed due to outstanding advantages in terms of easy processability, light weight, and excellent mechanical properties.[2,3]

Electrically conductive polymer-based composite materials with mobile charge carriers can interact with incident electromagnetic waves, and the EMI SE is positively related to the electrical conductivity.[4,5] Due to the excellent electrical conductivity, metal-based fillers are incorporated into the polymer matrix via physical and chemical methods.[5−7] The shape and loading content of metals in the polymer matrix play an important role in adjusting the EMI SE of the composites. For example, Joseph and Thomas Sebastian[8] added carbonyl iron particles (CIPs) of spherical shape into a polyvinylidene fluoride (PVDF) matrix to achieve a shielding effectiveness of about 20 dB in the X band for the PVDF−50 vol % CIP composite. However, a large amount of particle fillers is not desirable because it will form a stress concentration zone and deteriorate the mechanical reliability. To reduce metal consumption, Sundararaj et al.[9] mixed one-dimensional (1D) copper nanowires (CuNWs) into polystyrene (PS) to obtain composites with 2.1 vol % CuNWs, of which the EMI SE achieved was 35 dB. However, copper is readily oxidized under atmospheric conditions, and thus, for the advantage of greater resistance to oxidation, silver has gained a tremendous interest.[10] For example, Zeng et al.[11] prepared polyurethane/

Received: January 20, 2022
Accepted: March 16, 2022
Published: March 25, 2022

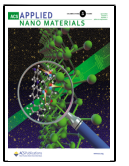

https://doi.org/10.1021/acsanm.2c00315
ACS Appl. Nano Mater. 2022, 5, 5292−5301

silver nanowire (AgNW) nanocomposites containing 28.6 wt %/0.152 vol % AgNWs, and the EMI SE reached 64 dB. Fan et al.[12] utilized the two-dimensional (2D) metal flake Ag nanosheets (AgNSs) to blend with epoxy. When the AgNS content was 30.0 wt %, the EMI SE value for the ultimate product was 49.7 dB. However, to obtain a desirable shielding property, the dosage of metal is still relatively large, and the cost for AgNWs as well as AgNSs is high. Considering economic feasibility and advantageous performances, choosing metal-based fillers with appropriate shapes to fabricate composites achieving high EMI SE at lower metal loading remains a challenge.

The distribution of fillers in the polymer matrix also determines the shielding performance. The formation of a three-dimensional (3D) segregated structure is favorable for enhancing the electrical conductivity and EMI shielding performances.[13−16] To date, many methods including dry or solution mixing, emulsion blending, melt blending, and electrostatic assembly strategies have been exploited to accomplish the goal of the abovementioned structure.[14,15] For example, Gelves[17] obtained films with a segregated nanowire network by mixing CuNWs in a miscible solvent mixture and treating with precipitation followed by annealing in a compression molder. Mamunya et al.[18] created a segregated structure consisting an ordered distribution of carbon nano- and microfillers within an ultrahigh-molecular-weight polyethylene matrix via a hot compacting method. Sun et al.[15] utilized electrostatic assembly to prepare MXene@PS hybrids, followed by compression molding into nanocomposites with a 3D segregated structure at 130 °C under 500 MPa. Nevertheless, these methods always require an ultrahigh pressure and a particular temperature or complicated procedures and are not suitable for large-scale production.[16] It is still challenging to develop a facile and energy-efficient strategy to control the distribution of fillers in polymer-based electromagnetic shielding composite materials with a segregated conductive network.

Recently, the state-of-the-art flexible electronics urgently needs materials not only possessing remarkable EMI SE but also exhibiting a suitable thickness.[2,19−22] Numerous studies have attempted to promote the EMI SE by increasing the thickness of the product. For example, Yu[23] found that when the thickness of the products was only 0.7 mm, it exhibited an EMI SE of approximately 25.0 dB. With the increment of thickness to 2 mm, the EMI SE would ascend monotonically and could reach 43.5 dB. However, the increment of thickness will not only result in heavy weight and loss of portability but also deteriorate the flexibility, which will greatly limit practical applications as flexible EMI shielding materials.[24] Improving the EMI SE of films per unit thickness, which is labeled as SE/d, has become an important topic. The investigation of a reasonable structural design to improve SE/d is worth exploring to meet the requirements of next-generation electronics.

In this work, to reduce the consumption of the metal and inspired by the prominent electrical conductivity of Ag nanoparticles, Ag nanoparticle-coated PS (PS@Ag) microspheres with a large PS core were designed as electrically conductive fillers, and the metallic shell constituting Ag nanoparticles could provide an efficient path for electron transfer. Taking advantage of the gravity-driven effect, a facile and energy-efficient strategy to control the distribution of PS@Ag microspheres in poly(vinyl alcohol) (PVA) was exploited from a spontaneous process to build a segregated laminar structure possessing an efficient 3D conductive network. Due to the volume exclusion effect[25] of big PS@Ag microspheres, composite films possessing an interconnected conductive network were fabricated with low silver loading. An only 0.1 mm flexible composite film with 6.3 wt % silver exhibited outstanding SE/d, reaching 243 dB/mm. To further investigate the effect of the structure on the EMI SE efficiency, films with the same thickness were fabricated through direct casting and multipiece stacking methods. For identical 0.3 mm thickness, the EMI SE of a three-piece stacking film reached 55.3 dB, which showed unique superiority compared to the triple-thickness casting film (37.2 dB). The facile processability for thin films with tailored satisfactory EMI SE by tuning the layer number through stacking at low metal loading makes it a promising way to design shielding materials for next-generation electronics.

EXPERIMENTAL METHODS

Materials. Ag nanoparticle-coated PS microspheres labeled as PS@Ag with a density of approximately 2 g/cm^3 were purchased from ZhongKe YuanZhen Technical Company (China). The corresponding precursor reagents including PS microspheres (average diameter was 2.5 μm, the coefficient of variation of microsphere size, C.V. = 0.008, as displayed in Figure S1 in the Supporting Information) and sensitized PS were supplied by the same company. PVA (CAS no.: 9002-89-5; polymerization degree of 1700, alcoholysis degree of 99%, purity >98%) was purchased from Aladdin Reagent Co., Ltd. Spherical Ag powder (purity ≥ 99.9%, average diameter was 350 nm) was provided by Ningbo Jin Lei Nano Mstar Technology Ltd. (China). Deionized water was prepared using a Milli-Q water purification system.

Fabrication of the PVA/PS@Ag Composite Film. A schematic diagram of the composite film is illustrated in Figure 1. The preparation process for PS@Ag mainly included coarsening, sensitizing, and reducing silver precursor ions. 5 g of PVA was mixed with 95 mL of water, heated at 95 °C for 3 h, and then cooled to obtain 5 wt % PVA solution for further use. To fabricate the PVA/PS@Ag film, a certain volume of 5 wt % PVA solution was blended with 8 mg/mL PS@Ag via sonification for 30 min. The mixture was cast in a Petri dish to volatilize water for 1 week at ambient temperature and dried in a vacuum oven at 40 °C for 24 h before characterization. As depicted in Table 1, a flexible 0.1 mm thick film (flexibility was confirmed, as depicted in Figure S2 in the Supporting Information) from a 2.5 mL mixture was obtained and labeled as the single-thickness casting film (CF-1). If the double volume mixture was directly poured in the Petri dish, the double-thickness casting film (CF-2) was acquired. For the purpose of preparing the double-piece stacking film (SF-2), one can stack two layers of CF-1. Following this analogy, the triple-thickness

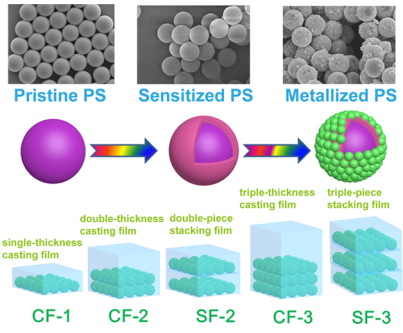

Figure 1. Schematic diagram for the fabrication of the film. CF-1, CF-2, and CF-3 are cast as one-piece films with different thicknesses. SF-2 and SF-3 are obtained by stacking different numbers of layers of CF-1.

https://doi.org/10.1021/acsanm.2c00315
ACS Appl. Nano Mater. 2022, 5, 5292−5301

Table 1. Description of the Composite Films with 8 mg/mL PS@Ag

type	dosage of PVA solution (mL)	thickness (mm)
CF-1	2.5	0.1
CF-2	5.0	0.2
SF-2	5.0	0.2
CF-3	7.5	0.3
SF-3	7.5	0.3

casting film (CF-3) was obtained via direct solution casting with a 3-fold volume mixture, and a triple-piece stacking film (SF-3) was obtained by stacking three layers of CF-1.

Characterization. The morphology of the composite film was characterized using the scanning electron microscopy (SEM) function of the focused ion beam (FIB Dual Beam System, Auriga, Zeiss, Germany). Core−shell PS@Ag was cut using FIB at 30 kV and 20 pA for 40 s. The structure of PS@Ag was studied using a JEM-2100 transmission electron microscope (JEOL, Ltd.) at an accelerating voltage of 100 kV and a Philips X'Pert Pro MPD X-ray diffractometer with Cu Kα radiation(λ = 0.154 nm, 40 kV, 40 mA). The elemental distribution of the samples was detected using an energy-dispersive spectroscopy (EDS) detector in a scanning electron microscope. The chemical composition of the samples was analyzed using X-ray photoelectron spectroscopy (XPS, ESCALAB 250Xi, Thermo Fisher). The loading amount of silver in PS@Ag was measured using a Q50 thermogravimetry analysis (TGA) apparatus in a nitrogen atmosphere at a heating rate of 10 °C/min from 30 to 700 °C. The thickness of the composite film was recorded using a digital thickness meter. The electrical conductivity was measured using a four-point probe meter (RTS-9, 4 Probes Technologies Inc, China), and each sample was measured five times to obtain the average value. Composite films were integrated into a homemade light-emitting diode (LED) lamp (3 W) device to certify its conductivity. Mechanical properties of composite films were characterized using an electronic universal testing machine (TY-5000, Yangzhou Tianyou Instrument Equipment Co. Ltd., China) with a stretching rate of 3 mm/min, and the size of rectangular samples was 30 mm × 3 mm. The EMI SE of the samples was measured in the frequency range of 8.2−12.4 GHz (X-band) at room temperature using a vector network analyzer (model MS46322B, Anritsu Technologies Inc. Japan). The waveguide measurement arrangement was adopted. The samples should be sandwiched by the holders tightly, and the space between the layers could be eliminated for stacking films. Electromagnetic radiation was incident from the PS@Ag side, and scattering parameters (S_{11} and S_{21}) were collected for further investigation. Based on the following equations, the power coefficients of reflectivity (R), transmissivity (T), and absorptivity (A) as well as the shielding effectiveness of total EMI SE (SE_T), absorption loss (SE_A), and reflection loss (SE_R) could be calculated.[26]

$$R = |S_{11}|^2$$

$$T = |S_{21}|^2$$

$$A = 1 - R - T$$

$$SE_R = -10 \log(1 - R)$$

$$SE_A = -10 \log[T/(1 - R)]$$

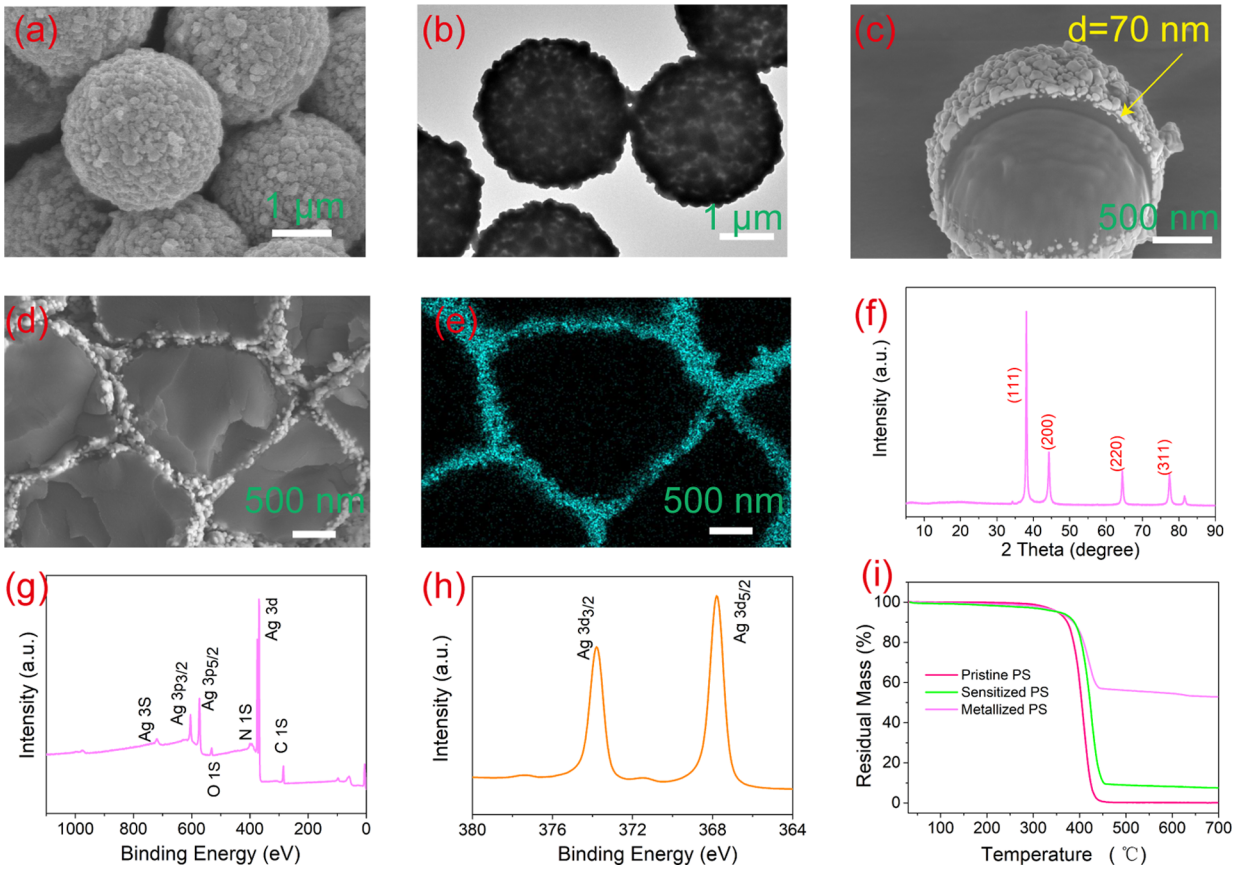

Figure 2. Characterization of PS@Ag. (a) SEM image of PS@Ag; (b) TEM image of PS@Ag; (c) FIB image of PS@Ag; (d) SEM image of cross-sectional PS@Ag composite tablets; (e) EDS elemental mapping image of Ag for cross-sectional PS@Ag composite tablets; (f) XRD patterns of PS@Ag; (g) XPS wide-scan spectrum of PS@Ag; (h) Ag 3d core-level spectrum of PS@Ag; and (i) TGA curves of pristine PS, sensitized PS, and PS@Ag.

https://doi.org/10.1021/acsanm.2c00315
ACS Appl. Nano Mater. 2022, 5, 5292−5301

$$SE_T = -10 \log T$$

RESULTS AND DISCUSSION

Characterization of PS@Ag Microspheres. According to the description of metallized PS particles from ZhongKe YuanZhen Technical Company (China), electroless plating was operated on the sensitized PS to achieve the core−shell structured product, and the loading of silver on PS microspheres was regulated by the concentration of silver precursor ions. The published literature reveals that sensitized PS microspheres could provide active sites for silver electroless deposition.[27] As illustrated in Figure 2a, the diameter of metallized PS was approximately 2.6 μm. A dense and uniform coverage of the silver shell on the PS surface could be found (Figure 2a,b), and it was attributed to Ag nanoparticle coating. The thickness of the silver shell was detected using the FIB, and it was nearly 70 nm (Figure 2c). The metallic shell composed of Ag nanoparticles was capable of providing an efficient path for electron transfer, and the metallized PS showed great potential as electrically conductive fillers. Composite tablets were obtained by compressing PS@Ag microspheres under 5 MPa at room temperature, and the electrical conductivity of composite tablets was 714 S/cm. The reason for such a high electrical conductivity was explored via SEM and EDS elemental mapping images of cross-sectional composites tablets. As depicted in Figure 2d,e, Ag nanoparticle-coated PS microspheres were deformed to interlock against the surface, and an effective electrically conductive path was confirmed to be built with a continuous silver shell. Furthermore, PS@Ag microspheres were characterized using X-ray diffraction (XRD) and XPS. As shown in Figure 2f, the characteristic peaks at 2θ = 38.10, 44.32, 64.46, and 77.40° corresponded to the (111), (200), (220), and (311) faces of the face-centered cubic structure of silver, respectively.[28] The strong signal peak for the binding energy around 370.0 eV in the XPS wide-scan data belonged to Ag_{3d} from metallic silver (Figure 2g).[29,30] The zero-valent metallic silver was further certified by the Ag 3d core-level spectrum of PS@Ag microspheres, as displayed in Figure 2h. It consisted of two peaks at binding energies of 368.0 and 374.0 eV corresponding to Ag $3d_{5/2}$ and Ag $3d_{3/2}$, respectively.[29] Both peaks were assigned to Ag^0 species, thus verifying the existence of Ag, which was in accordance with XRD results. To calculate the Ag content of PS@Ag microspheres, TGA was employed to investigate the loading amount of Ag, as shown in Figure 2i. The residual weights of pure PS, sensitized PS, and metallized PS microspheres were 0.12, 7.54, and 52.88 wt %, respectively. Through subtraction, the weight fraction of Ag content in PS@Ag microspheres was determined to be 45.34%.

Characterization of the Composite Film. A single-thickness casting film (CF-1) with a thickness of approximately 0.1 mm was obtained and characterized, as shown in Figure 3a. The thicknesses of other casting films are recorded in Figure S3 in the Supporting Information. The density of the core−shell PS@Ag microspheres was approximately 2 g/cm^3. When core−shell PS@Ag microspheres were mixed with 5 wt % PVA solution, followed by evaporation at room temperature for 1 week, with the assistance of gravity and the volume exclusion effect, sedimentation occurred, and the PS@Ag microspheres were connected with each other to construct a laminated and segregated conductive network. The sedimentation of PS@Ag microspheres could also be confirmed via SEM of the cross-sectional film. One could clearly find the existence of a boundary between fillers and the PVA matrix (shown in Figure 3b). Such a laminated structure resulted in the different conductivities of both sides. As illustrated in Figure 3c,d, the bottom side assembled with PS@Ag microspheres connected with each other could light the LED lamp, while the top side failed to do so. This revealed that a conductive network was formed at the bottom side, which could supply an effective electron transfer channel. The detailed electrically conductive network was further confirmed by magnified SEM and EDS elemental mapping images of Ag of the cross-sectional composite film. As shown in Figure 3e,f, the adjacent silver shells connect with each other along the interfaces to form a consecutive and well-defined 3D network. Such a 3D conductive network could guarantee the effective migration of electrons,[15,16] and the corresponding electrical conductivity for CF-1 could reach 10.6 s/cm.

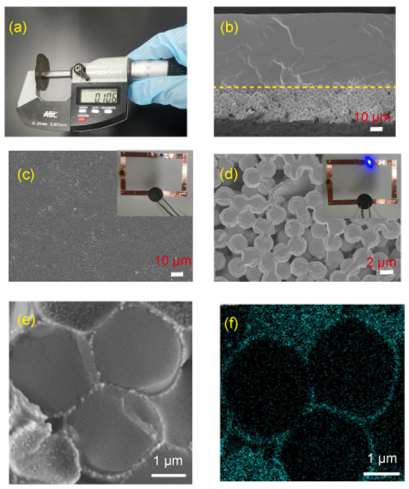

Figure 3. Characterization of the composite film. (a) Thickness measurement of CF-1; (b) SEM image of the cross-section of CF-1; (c) SEM image of top side of CF-1 (the inset shows nonconduction); (d) SEM image of the bottom side of CF-1 (the inset shows conduction); (e) magnified SEM image of the cross-section of CF-1; and (f) EDS elemental mapping image of Ag in the cross-section of CF-1.

To further investigate the effect of filler loading on the structure of films, three concentrations of 2, 8, and 12 mg/mL of PS@Ag were taken into consideration to fabricate a single-thickness film. As exhibited in Figure 4a1,2, due to the tiny amount of PS@Ag at 2 mg/mL, most of the PS@Ag microspheres sank to the bottom of the film, but some microspheres could not link with each other. The counterpart Ag powders with equivalent silver weights with respect to the corresponding concentration of PS@Ag were incorporated into PVA solution for comparison (explicated in Figure 4a3,4), and scattered silver particles that could not form an electrical conductivity network could be found. With the increment of PS@Ag concentration to 8 mg/mL, a perfect segregated and laminated structured film was formed, and the silver coating joined together to build an effective conductive path (shown in Figure 4b1,2). However, faultage existed at the filler area in the film with equivalent silver weight for Ag powder (displayed in Figure 4b3,4). Upon further increasing the PS@Ag concentration to 12 mg/mL, the network for the silver coating could be clearly observed, as shown in Figure 4c1,2. These conductive networks are beneficial for boosting the EMI SE,

https://doi.org/10.1021/acsanm.2c00315
ACS Appl. Nano Mater. 2022, 5, 5292−5301

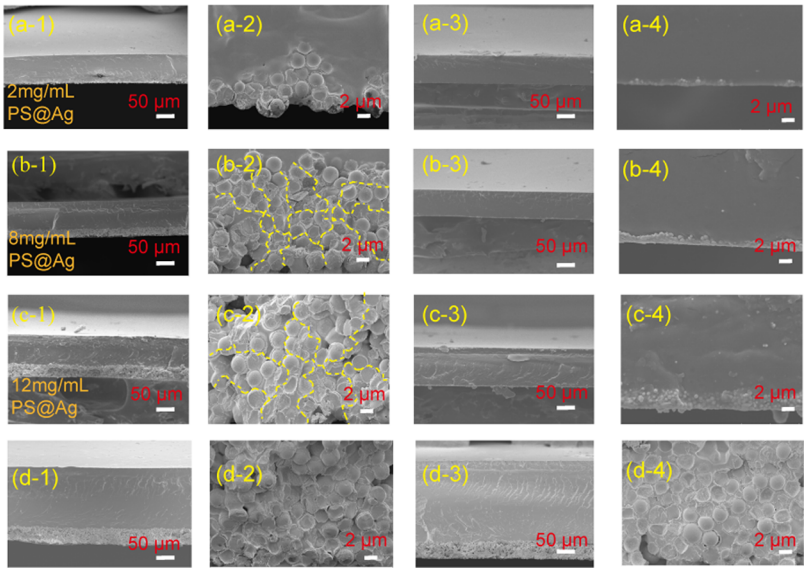

Figure 4. Characterization of the composite film. SEM images of the cross-section of the single-thickness casting film for 2 mg/mL PS@Ag (a-1,a-2) and corresponding Ag powder (a-3,a4); 8 mg/mL PS@Ag (b-1,b-2) and corresponding Ag powder (b-3,b-4); and 12 mg/mL PS@Ag (c-1,c-2) and corresponding Ag powder (c-3,c-4). SEM images of the cross-section of the film for CF-2 (d-1,d-2) and CF-3 (d-3,d-4).

which is discussed in the following section. However, numerous gaps between particles impeded the effective contact of particles for the equivalent silver content of Ag powders (shown in Figure 4c3,4). It was concluded that the large PS core in the core−shell PS@Ag microspheres guaranteed the construction of an electrically conductive network at low silver loading. To further investigate the structure affecting the SE efficiency, CF-2 (Figure 4d1,2) and CF-3 (Figure 4d3,4) were obtained with a single sedimentary filler layer at the bottom of the film, which is compared to the alternate layers for the stacking film in the subsequent section. The information of mechanical properties and mechanical durability of composite films could be found in the Supporting Information.

Comparison between Core−shell PS@Ag and Ag Powder as Fillers in Terms of EMI SE. As shown in Figure 5a, during the X-band (frequency range of 8.2−12.4 GHz), the average EMI SE of the films increased from 13.8 to 24.3 and to 26.5 dB with 2, 8, and 12 mg/mL PS@Ag in the single-thickness film. By converting to mass fraction, the silver loading values are 1.7, 6.3, and 8.8 wt %, respectively. The EMI SE increases significantly from 2 to 8 mg/mL but slightly from 8 to 12 mg/mL. Based on the percolation theory,[31] the percolation threshold is approximately 8 mg/mL. It is noteworthy that an average EMI SE of 24.3 dB in the X-band could be achieved with only 8 mg/mL metallized PS microspheres in the PVA film at merely 0.1 mm, already meeting the need for commercial application for shielding effectiveness (20 dB).[32] To explore the superiority of PS@Ag as a conductive filler, comparison experiments were carried out utilizing Ag powder with the equivalent silver weight during the fabrication of films. As displayed in Figure 5a, the average EMI SE for films consisting of Ag powder was only 0.2, 3.1, and 8.3 dB with respect to the equivalent silver contents for PS@Ag of 2, 8, and 12 mg/mL, respectively, which cannot satisfy the commercial requirement. Obviously, the utilization of PS@Ag as a filler for EMI SE is superior to Ag powder.

The difference between PS@Ag and Ag powder in term of EMI SE is mainly ascribed to the following reasons. For Ag powder (explicated in Figure 5b), ascribed to the impedance mismatch, reflection of electromagnetic radiation existed based on the interaction of incident waves with free electrons on the surface of interconnected conductive particles.[33] The penetrating waves stimulate the charge carriers to migrate and generate heat, leading to Ohmic loss and attenuation of the energy of electromagnetic radiation.[22,34,35] However, for the core−shell structured PS@Ag, Ag nanoparticles were deposited on the surface of PS microspheres with a large core (2.5 μm), and the shielding mechanism were of four types (displayed in Figure 5c). Similar to the Ag powder, impedance mismatch and Ohmic loss existed in PS@Ag microspheres. In addition, for the individual core−shell PS@Ag, interfacial polarization would occur at the boundary between the core and the shell due to confined space charges at the interfaces.[22,36,37] Herein, the insulating PS core and conductive Ag coating introduce multiple interfaces that could generate bound charges at the interfaces, causing the polarization effect. The interfacial polarization would endeavor to attenuate electromagnetic energy via dielectric loss.[22] Moreover, the large number of interfaces could supply additional active sites for scattering and multiple internal reflections of EM waves .[22] Under the assistance of gravity and taking advantage of core−shell structured PS@Ag with a large core, high EMI SE could be achieved due to synergistic effects of electric migration/interfacial polarization/multiple internal reflections and scatterings at low silver loading with a combination of segregated and laminated structures in the films.

Effect of Multiple Interfaces in Films on EMI SE. To investigate the effect of multiple interfaces in films with the same thickness on EMI SE, the products were fabricated via direct casting and stacking processes with a PS@Ag concentration of 8 mg/mL, as shown in Figure 5d. The average EMI SE_T values for CF-2 and SF-2 are 33.5 and 39.9 dB, respectively. For CF-3 and SF-3, the average EMI SE_T values are 37.2 and 55.3 dB, respectively. With the same thickness, the multipiece stacking film has a higher SE_T than the multithickness casting film over the whole X-band frequency range. The SE_R and SE_A are presented in Figure 5e. The results indicate that with the increment of film

https://doi.org/10.1021/acsanm.2c00315
ACS Appl. Nano Mater. 2022, 5, 5292−5301

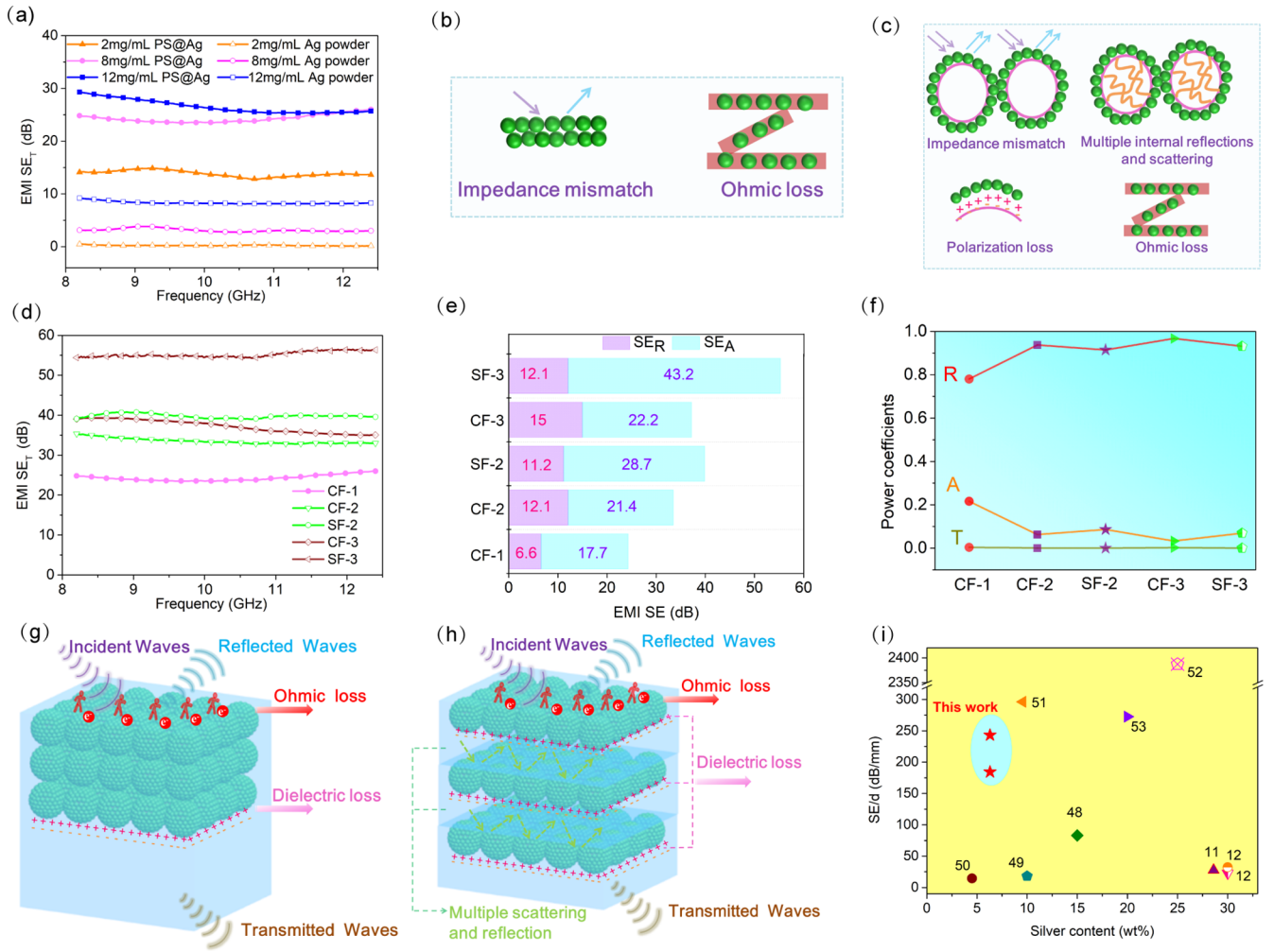

Figure 5. EMI SE of the composite film. (a) Comparison of EMI SE between PS@Ag and corresponding equivalent silver weight for Ag powder; (b) shielding mechanism of EMI SE for Ag powder; (c) shielding mechanism of EMI SE for core−shell PS@Ag; (d) EMI SE of the composite films with different structures; (e) SE_R and SE_A for composite films; (f) power coefficients for composite films; (g) shielding mechanism of EMI SE for casting films; (h) shielding mechanism of EMI SE for stacking films; (i) comparison of EMI SE values for PVA/PS@Ag composites (marked as red stars) with those of other reported literature studies. SE/*d* is depicted as EMI SE_T per unit thickness. Numbers inside the plot correspond to the reference information listed in Table 2.

thickness from 0.1 to 0.2 and to 0.3 mm, an obvious increment of absorption loss for the stacking film could be found, reaching 17.7, 28.7, and 43.2 dB, respectively. However, for the casting film, absorption loss increases indistinctively, and the values are 17.7, 21.4, and 22.2 dB, respectively. This shows that the existence of multiple interfaces is in favor of enhancing SE_A. It is worth noting that though the values of SE_A are larger than SE_R, it does not indicate that the composite films are absorption-dominant shielding materials.[38−40] SE_R and SE_A are relative quantities and are not related with the absolute power value.[38] The power coefficients *A* and *R* are quantitative characteristics of power balance when an electromagnetic wave is incident on a shielding material.[38] Some inconsistent phenomena between *A* and SE_A have been reported,[38,40,41] but power coefficients are recommended to evaluate the dominant shielding mechanism.[39,42,43] As depicted in Figure 5f, the *R*, *A*, and *T* coefficients of composite films are computed. The values of *R* are larger than *A* for all composite films. This indicates that the dominant shielding mechanism for all samples is reflection. For CF-1, CF-2, and CF-3, the values of *R* gradually increase. The growing reflection is attributed to the stronger impedance mismatch with the increasing amount of conductive fillers in the thicker film. As for films with identical thickness, by comparing CF-2 and SF-2, it is found that *R* is lower but *A* is higher in the stacking film. The same trend can be found between CF-3 and SF-3. The greater value of *A* for stacking films confirms the advantage of multiple interfaces, which are beneficial to absorption of EMI waves.

To further investigate the shielding process in detail, the mechanisms of shielding for the multithickness casting film and multipiece stacking films (displayed in Figure 5g,h) are described as follows: (1) when the incident electromagnetic (EM) waves meet the films with 3D conductive networks, owing to the impedance mismatch between the air and surface of the shielding materials, a portion of EM waves is reflected back. Energy loss is generated by the electrons at the boundary, serving as mobile charge carriers to reflect the waves.[22,44] (2) The penetrated electromagnetic waves further interact with PS@Ag in conductive networks to be converted into thermal energy via Ohmic loss.[45] In addition, due to the large conductivity mismatch between the boundary of the

https://doi.org/10.1021/acsanm.2c00315
ACS Appl. Nano Mater. 2022, 5, 5292−5301

Table 2. Comparison of EMI SE_T per Unit Thickness at Different Mass Fractions of Silver for Composites in This Work and Previous Literature Studies

composites	EMI SE_T (dB)	thickness (mm)	SE/d (dB/mm)	content (wt %)	refs
PBZ/PrGO/AgNP	54	0.65	83.1	15	48
PVDF/CNT/AgNP	≈20	1.1	18.2	10	49
epoxy/carbon fiber/AgNP	35−38	2.5	14−15.2	4.5	50
PU/AgNW	64	2.3	27.8	28.6	11
PPy/PDA/AgNW	25.9	0.095	272.6	20	53
cellulose paper/AgNW	48.6	0.164	296.3	9.57	51
ANF/AgNW	56.1	0.0235	2387.2	25	52
epoxy foams/AgNS	49.7	2.18	22.8	30	12
epoxy/AgNS	35	1.08	32.4	30	12
PVA/PS@Ag	24.3	0.1	243	6.3	this work
PVA/PS@Ag	55.3	0.3	184.3	6.3	this work

interconnected PS@Ag layer and PVA, interfacial polarization can occur by plenty of dipoles, which would bring about dielectric loss.[46] For samples with identical thickness, the stacking films possess more conductivity mismatching interfaces, contributing to stronger dielectric loss. Furthermore, when the surviving electromagnetic waves encounter alternating conductive PS@Ag sides in the multipiece stacking film, the repeated internal reflection and scattering would convert electromagnetic waves into heat loss in the form of microcurrents, which is beneficial for enhancing the absorption of electromagnetic waves.[32,42] To sum up, alternating interfaces in the stacking film make a positive contribution to the promotion of absorption. It will undergo a particular "absorption−reflection−reabsorption" process in the stacking samples. In addition, the EMI SE of the composite films per unit thickness (SE/d) in this work is compared with the other public literature studies.[47−53] As presented in Table 2 and Figure 5i, at low silver loading, the films fabricated in this work exhibit outstanding SE/d, which is ascribed to the combination of core−shell structured fillers and reasonable structure design.

CONCLUSIONS

In summary, a facile and energy-efficient strategy to control the distribution of fillers in thin flexible film was exploited, and it was a self-driven process to form a segregated laminar structure via utilizing Ag nanoparticle-coated PS microspheres as conductive fillers in a PVA matrix. The silver shell composed of Ag nanoparticles could provide an effective electron migration channel to ensure high electrical conductivity. The volume exclusion effect guaranteed the construction of an electrically conductive network with low silver loading. Benefiting from the delicate structure, a merely 0.1 mm composite film exhibited remarkable SE/d, reaching 243 dB/mm with only 6.3 wt % silver loading. Moreover, the superiority of introducing multiple interfaces for enhancing shielding performance was confirmed by stacking films, in which the average EMI SE_T for triple-piece stacking films was 55.3 dB compared to 37.2 dB for the triple-thickness casting film. The multiple interfaces are beneficial to the absorption of EMI waves. Tuning of the EMI SE for the composites could be carried out by easily adjusting the stacking numbers of the composite film. Such a convenient method not only guarantees the tailored enhancement of EMI SE but also shows promising potential for large-scale applications.

ASSOCIATED CONTENT

Supporting Information

The Supporting Information is available free of charge at https://pubs.acs.org/doi/10.1021/acsanm.2c00315.

Size distribution of PS microspheres, flexibility of the single-thickness casting film (CF-1), thicknesses of casting films for CF-2 and CF-3, and mechanical properties and mechanical durability of composite films (PDF)

Bending−release cycle of CF-1 for mechanical durability analysis (MP4)

AUTHOR INFORMATION

Corresponding Authors

Yi Gong − *Key Laboratory of Photovolatic and Energy Conservation Materials, Institute of Solid State Physics, Hefei Institutes of Physical Science, Chinese Academy of Sciences (CASHIPS), Hefei 230031, People's Republic of China;* orcid.org/0000-0002-3721-2678; Email: yigong@rntek.cas.cn

Xingyou Tian − *Key Laboratory of Photovolatic and Energy Conservation Materials, Institute of Solid State Physics, Hefei Institutes of Physical Science, Chinese Academy of Sciences (CASHIPS), Hefei 230031, People's Republic of China;* Email: xytian@issp.ac.cn

Authors

Hua Cheng − *Key Laboratory of Photovolatic and Energy Conservation Materials, Institute of Solid State Physics, Hefei Institutes of Physical Science, Chinese Academy of Sciences (CASHIPS), Hefei 230031, People's Republic of China; University of Science and Technology of China, Hefei 230026, People's Republic of China; Department of Chemistry and Chemical Engineering, Hefei Normal University, Hefei 230061, People's Republic of China*

Siqi Liu − *Department of Structural Engineering, Faculty of Engineering, Norwegian University of Science and Technology (NTNU), 7491 Trondheim, Norway*

Ruiqi Wang − *University of Nottingham Ningbo China, 315100 Ningbo, People's Republic of China*

Wei Zhang − *Key Laboratory of Photovolatic and Energy Conservation Materials, Institute of Solid State Physics, Hefei Institutes of Physical Science, Chinese Academy of Sciences (CASHIPS), Hefei 230031, People's Republic of China*

Rui Pan − *Key Laboratory of Photovolatic and Energy Conservation Materials, Institute of Solid State Physics, Hefei Institutes of Physical Science, Chinese Academy of Sciences*

https://doi.org/10.1021/acsanm.2c00315
ACS Appl. Nano Mater. 2022, 5, 5292−5301

(CASHIPS), Hefei 230031, People's Republic of China; University of Science and Technology of China, Hefei 230026, People's Republic of China

Zhe Li − *Key Laboratory of Photovolatic and Energy Conservation Materials, Institute of Solid State Physics, Hefei Institutes of Physical Science, Chinese Academy of Sciences (CASHIPS), Hefei 230031, People's Republic of China; University of Science and Technology of China, Hefei 230026, People's Republic of China*

Fangkuo Wang − *Department of Chemistry and Chemical Engineering, Hefei Normal University, Hefei 230061, People's Republic of China*

Rui Hu − *Key Laboratory of Photovolatic and Energy Conservation Materials, Institute of Solid State Physics, Hefei Institutes of Physical Science, Chinese Academy of Sciences (CASHIPS), Hefei 230031, People's Republic of China;* orcid.org/0000-0001-7799-5198

Jianjun Ding − *Key Laboratory of Photovolatic and Energy Conservation Materials, Institute of Solid State Physics, Hefei Institutes of Physical Science, Chinese Academy of Sciences (CASHIPS), Hefei 230031, People's Republic of China;* orcid.org/0000-0002-7597-2141

Xian Zhang − *Key Laboratory of Photovolatic and Energy Conservation Materials, Institute of Solid State Physics, Hefei Institutes of Physical Science, Chinese Academy of Sciences (CASHIPS), Hefei 230031, People's Republic of China;* orcid.org/0000-0002-7910-1562

Chen Lin − *Key Laboratory of Photovolatic and Energy Conservation Materials, Institute of Solid State Physics, Hefei Institutes of Physical Science, Chinese Academy of Sciences (CASHIPS), Hefei 230031, People's Republic of China*

Jianying He − *Department of Structural Engineering, Faculty of Engineering, Norwegian University of Science and Technology (NTNU), 7491 Trondheim, Norway;* orcid.org/0000-0001-8485-7893

Complete contact information is available at: https://pubs.acs.org/10.1021/acsanm.2c00315

Notes

The authors declare no competing financial interest.

■ ACKNOWLEDGMENTS

The authors gratefully acknowledge the financial supports from the Youth Innovation Promotion Association CAS (grant no. 2020446); the CASHIPS Director's Fund (grant nos: YZJJZX202015 and YZJJ202102); the Anhui Provincial Natural Science Foundation (1908085QB64); The Natural Science Foundation of the Education Department of Anhui Province (KJ2019A0731 and KJ2021A0919); the Key Lab of Photovoltaic and Energy Conservation Materials, CAS; the Anhui Province Key Laboratory of Environment-friendly Polymer Materials; and the special project for the construction of the biological medicine and electronic information platform of Hefei Normal University.

■ REFERENCES

(1) Yao, B.; Hong, W.; Chen, T.; Han, Z.; Xu, X.; Hu, R.; Hao, J.; Li, C.; Li, H.; Perini, S. E.; Lanagan, M. T.; Zhang, S.; Wang, Q.; Wang, H. Highly Stretchable Polymer Composite with Strain-Enhanced Electromagnetic Interference Shielding Effectiveness. *Adv. Mater.* **2020**, *32*, 1907499.

(2) Sankaran, S.; Deshmukh, K.; Ahamed, M. B.; Khadheer Pasha, S. K. Recent advances in electromagnetic interference shielding properties of metal and carbon filler reinforced flexible polymer composites: A review. *Composites, Part A* **2018**, *114*, 49−71.

(3) Jiang, D.; Murugadoss, V.; Wang, Y.; Lin, J.; Ding, T.; Wang, Z.; Shao, Q.; Wang, C.; Liu, H.; Lu, N.; Wei, R.; Subramania, A.; Guo, Z. Electromagnetic Interference Shielding Polymers and Nanocomposites - A Review. *Polym. Rev.* **2019**, *59*, 280−337.

(4) Lee, S. H.; Yu, S.; Shahzad, F.; Hong, J. P.; Kim, W. N.; Park, C.; Hong, S. M.; Koo, C. M. Highly anisotropic Cu oblate ellipsoids incorporated polymer composites with excellent performance for broadband electromagnetic interference shielding. *Compos. Sci. Technol.* **2017**, *144*, 57−62.

(5) Wanasinghe, D.; Aslani, F. A review on recent advancement of electromagnetic interference shielding novel metallic materials and processes. *Composites, Part B* **2019**, *176*, 107207.

(6) Zhang, J.; Li, J.; Tan, G.; Hu, R.; Wang, J.; Chang, C.; Wang, X. Thin and Flexible Fe-Si-B/Ni-Cu-P Metallic Glass Multilayer Composites for Efficient Electromagnetic Interference Shielding. *ACS Appl. Mater. Interfaces* **2017**, *9*, 42192−42199.

(7) Xu, Z.; Hao, H. Electromagnetic interference shielding effectiveness of aluminum foams with different porosity. *J. Alloys Compd.* **2014**, *617*, 207−213.

(8) Joseph, N.; Thomas Sebastian, M. Electromagnetic interference shielding nature of PVDF-carbonyl iron composites. *Mater. Lett.* **2013**, *90*, 64−67.

(9) Al-Saleh, M. H.; Gelves, G. A.; Sundararaj, U. Copper nanowire/polystyrene nanocomposites: Lower percolation threshold and higher EMI shielding. *Composites, Part A* **2011**, *42*, 92−97.

(10) Arjmand, M.; Moud, A. A.; Li, Y.; Sundararaj, U. Outstanding electromagnetic interference shielding of silver nanowires: comparison with carbon nanotubes. *RSC Adv.* **2015**, *5*, 56590−56598.

(11) Zeng, Z.; Chen, M.; Pei, Y.; Seyed Shahabadi, S. I.; Che, B.; Wang, P.; Lu, X. Ultralight and Flexible Polyurethane/Silver Nanowire Nanocomposites with Unidirectional Pores for Highly Effective Electromagnetic Shielding. *ACS Appl. Mater. Interfaces* **2017**, *9*, 32211−32219.

(12) Fan, X.; Zhang, G.; Gao, Q.; Li, J.; Shang, Z.; Zhang, H.; Zhang, Y.; Shi, X.; Qin, J. Highly expansive, thermally insulating epoxy/Ag nanosheet composite foam for electromagnetic interference shielding. *Chem. Eng. J.* **2019**, *372*, 191−202.

(13) Zhang, X.-P.; Jia, L.-C.; Zhang, G.; Yan, D.-X.; Li, Z.-M. A highly efficient and heat-resistant electromagnetic interference shielding carbon nanotube/poly(phenylene sulfide) composite via sinter molding. *J. Mater. Chem. C* **2018**, *6*, 10760−10766.

(14) Wang, M.; Tang, X.-H.; Cai, J.-H.; Wu, H.; Shen, J.-B.; Guo, S.-Y. Construction, mechanism and prospective of conductive polymer composites with multiple interfaces for electromagnetic interference shielding: A review. *Carbon* **2021**, *177*, 377−402.

(15) Sun, R.; Zhang, H.-B.; Liu, J.; Xie, X.; Yang, R.; Li, Y.; Hong, S.; Yu, Z.-Z. Highly Conductive Transition Metal Carbide/Carbonitride-(MXene)@polystyrene Nanocomposites Fabricated by Electrostatic Assembly for Highly Efficient Electromagnetic Interference Shielding. *Adv. Funct. Mater.* **2017**, *27*, 1702807.

(16) Wang, L.; Ma, Z.; Zhang, Y.; Chen, L.; Cao, D.; Gu, J. Polymer-based EMI shielding composites with 3D conductive networks: A mini-review. *SusMat* **2021**, *1*, 413−431.

(17) Gelves, G. A.; Al-Saleh, M. H.; Sundararaj, U. Highly electrically conductive and high performance EMI shielding nanowire/polymer nanocomposites by miscible mixing and precipitation. *J. Mater. Chem.* **2011**, *21*, 829−836.

(18) Mamunya, Y.; Matzui, L.; Vovchenko, L.; Maruzhenko, O.; Oliynyk, V.; Pusz, S.; Kumanek, B.; Szeluga, U. Influence of conductive nano- and microfiller distribution on electrical conductivity and EMI shielding properties of polymer/carbon composites. *Compos. Sci. Technol.* **2019**, *170*, 51−59.

(19) Yin, G.; Wang, Y.; Wang, W.; Qu, Z.; Yu, D. A Flexible Electromagnetic Interference Shielding Fabric Prepared by Construction of PANI/MXene Conductive Network via Layer-by-Layer Assembly. *Adv. Mater. Interfaces* **2021**, *8*, 2001893.

(20) Choi, H. Y.; Lee, T.-W.; Lee, S.-E.; Lim, J.; Jeong, Y. G. Silver nanowire/carbon nanotube/cellulose hybrid papers for electrically conductive and electromagnetic interference shielding elements. *Compos. Sci. Technol.* **2017**, *150*, 45−53.
(21) Liu, L. X.; Chen, W.; Zhang, H. B.; Wang, Q. W.; Guan, F.; Yu, Z. Z. Flexible and Multifunctional Silk Textiles with Biomimetic Leaf-Like MXene/Silver Nanowire Nanostructures for Electromagnetic Interference Shielding, Humidity Monitoring, and Self-Derived Hydrophobicity. *Adv. Funct. Mater.* **2019**, *29*, 1905197.
(22) Bhattacharjee, Y.; Bose, S. Core−Shell Nanomaterials for Microwave Absorption and Electromagnetic Interference Shielding: A Review. *ACS Appl. Nano Mater.* **2021**, *4*, 949−972.
(23) Yu, W.-C.; Wang, T.; Liu, Y.-H.; Wang, Z.-G.; Xu, L.; Tang, J.-H.; Dai, K.; Duan, H.-J.; Xu, J.-Z.; Li, Z.-M. Superior and highly absorbed electromagnetic interference shielding performance achieved by designing the reflection-absorption-integrated shielding compartment with conductive wall and lossy core. *Chem. Eng. J.* **2020**, *393*, 124644.
(24) Zeng, Z.; Chen, M.; Jin, H.; Li, W.; Xue, X.; Zhou, L.; Pei, Y.; Zhang, H.; Zhang, Z. Thin and flexible multi-walled carbon nanotube/waterborne polyurethane composites with high-performance electromagnetic interference shielding. *Carbon* **2016**, *96*, 768−777.
(25) Wu, K.; Wu, L.; Yang, W.; Chai, S.; Chen, F.; Fu, Q. Largely enhanced electrical properties of polymer composites via the combined effect of volume exclusion and synergy. *RSC Adv.* **2016**, *6*, 51900−51907.
(26) Sheng, A.; Ren, W.; Yang, Y.; Yan, D.-X.; Duan, H.; Zhao, G.; Liu, Y.; Li, Z.-M. Multilayer WPU conductive composites with controllable electro-magnetic gradient for absorption-dominated electromagnetic interference shielding. *Composites, Part A* **2020**, *129*, 105692.
(27) Wang, C.-J.; Hung, P.-S.; Chou, S.-C.; Chung, W.-A.; Wu, P.-W. Synthesis of polystyrene@polypyrrole-COOH@Ag (core@shell@shell) microspheres for potential application in anisotropic conductive paste. *Mater. Lett.* **2020**, *263*, 127239.
(28) Ma, Y.; Zhang, Q. Preparation and characterization of monodispersed PS/Ag composite microspheres through modified electroless plating. *Appl. Surf. Sci.* **2012**, *258*, 7774−7780.
(29) Cong, Y.; Xia, T.; Zou, M.; Li, Z.; Peng, B.; Guo, D.; Deng, Z. Mussel-inspired polydopamine coating as a versatile platform for synthesizing polystyrene/Ag nanocomposite particles with enhanced antibacterial activities. *J. Mater. Chem. B* **2014**, *2*, 3450−3461.
(30) Lu, Y.; He, Y.; Li, Y.; Xue, J.; Liu, H.; Cheng, B.; Li, X. Silver-plated polyamide fabrics with high electromagnetic shielding effectiveness performance prepared by in situ reduction of polydopamine and chemical silvering. *J. Appl. Polym. Sci.* **2019**, *136*, 48227.
(31) Kruželák, J.; Kvasničáková, A.; Hložeková, K.; Hudec, I. Progress in polymers and polymer composites used as efficient materials for EMI shielding. *Nanoscale Adv.* **2021**, *3*, 123−172.
(32) Wang, L.; Song, P.; Lin, C. T.; Kong, J.; Gu, J. 3D Shapeable, Superior Electrically Conductive Cellulose Nanofibers/Ti_3C_2Tx MXene Aerogels/Epoxy Nanocomposites for Promising EMI Shielding. *Research* **2020**, *2020*, 4093732.
(33) Wang, L.; Qiu, H.; Liang, C.; Song, P.; Han, Y.; Han, Y.; Gu, J.; Kong, J.; Pan, D.; Guo, Z. Electromagnetic interference shielding MWCNT-Fe_3O_4@Ag/epoxy nanocomposites with satisfactory thermal conductivity and high thermal stability. *Carbon* **2019**, *141*, 506−514.
(34) Lu, M.; Wang, X.; Cao, W.; Yuan, J.; Cao, M. Carbon nanotube-CdS core-shell nanowires with tunable and high-efficiency microwave absorption at elevated temperature. *Nanotechnol* **2016**, *27*, 065702.
(35) Zhang, Y.; Ruan, K.; Gu, J. Flexible Sandwich-Structured Electromagnetic Interference Shielding Nanocomposite Films with Excellent Thermal Conductivities. *Small* **2021**, *17*, 2101951.
(36) Chen, Y.-J.; Xiao, G.; Wang, T.-S.; Ouyang, Q.-Y.; Qi, L.-H.; Ma, Y.; Gao, P.; Zhu, C.-L.; Cao, M.-S.; Jin, H.-B. Porous Fe_3O_4/Carbon Core/Shell Nanorods: Synthesis and Electromagnetic Properties. *J. Phys. Chem. C* **2011**, *115*, 13603−13608.
(37) Liu, P.; Gao, S.; Wang, Y.; Huang, Y.; Wang, Y.; Luo, J. Core-Shell CoNi@Graphitic Carbon Decorated on B,N-Codoped Hollow Carbon Polyhedrons toward Lightweight and High-Efficiency Microwave Attenuation. *ACS Appl. Mater. Interfaces* **2019**, *11*, 25624−25635.
(38) Xu, Y.; Yang, Y.; Duan, H.; Gao, J.; Yan, D.-X.; Zhao, G.; Liu, Y. Flexible and highly conductive sandwich nylon/nickel film for ultra-efficient electromagnetic interference shielding. *Appl. Surf. Sci.* **2018**, *455*, 856−863.
(39) Peng, M.; Qin, F. Clarification of basic concepts for electromagnetic interference shielding effectiveness. *J. Appl. Phys.* **2021**, *130*, 225108.
(40) Zhang, L.; Luo, J.; Zhang, S.; Yan, J.; Huang, X.; Wang, L.; Gao, J. Interface sintering engineered superhydrophobic and durable nanofiber composite for high-performance electromagnetic interference shielding. *J. Mater. Sci. Technol.* **2022**, *98*, 62−71.
(41) Jung, J.; Lee, H.; Ha, I.; Cho, H.; Kim, K. K.; Kwon, J.; Won, P.; Hong, S.; Ko, S. H. Highly Stretchable and Transparent Electromagnetic Interference Shielding Film Based on Silver Nanowire Percolation Network for Wearable Electronics Applications. *ACS Appl. Mater. Interfaces* **2017**, *9*, 44609−44616.
(42) Zhang, Y.; Ruan, K.; Shi, X.; Qiu, H.; Pan, Y.; Yan, Y.; Gu, J. Ti_3C_2Tx/rGO porous composite films with superior electromagnetic interference shielding performances. *Carbon* **2021**, *175*, 271−280.
(43) Han, L.; Song, Q.; Li, K.; Yin, X.; Sun, J.; Li, H.; Zhang, F.; Ren, X.; Wang, X. Hierarchical, seamless, edge-rich nanocarbon hybrid foams for highly efficient electromagnetic-interference shielding. *J. Mater. Sci. Technol.* **2021**, *72*, 154−161.
(44) Fang, F.; Li, Y.-Q.; Xiao, H.-M.; Hu, N.; Fu, S.-Y. Layer-structured silver nanowire/polyaniline composite film as a high performance X-band EMI shielding material. *J. Mater. Chem. C* **2016**, *4*, 4193−4203.
(45) Liang, C.; Liu, Y.; Ruan, Y.; Qiu, H.; Song, P.; Kong, J.; Zhang, H.; Gu, J. Multifunctional sponges with flexible motion sensing and outstanding thermal insulation for superior electromagnetic interference shielding. *Composites, Part A* **2020**, *139*, 106143.
(46) Li, Y.; Shen, B.; Pei, X.; Zhang, Y.; Yi, D.; Zhai, W.; Zhang, L.; Wei, X.; Zheng, W. Ultrathin carbon foams for effective electromagnetic interference shielding. *Carbon* **2016**, *100*, 375−385.
(47) Jin, X.; Wang, J.; Dai, L.; Liu, X.; Li, L.; Yang, Y.; Cao, Y.; Wang, W.; Wu, H.; Guo, S. Flame-retardant poly(vinyl alcohol)/MXene multilayered films with outstanding electromagnetic interference shielding and thermal conductive performances. *Chem. Eng. J.* **2020**, *380*, 122475.
(48) Kumaran, R.; Kumar, A. V.; Ramaprabhu, S.; Subramanian, V. Absorption-enhanced EMI shielding using silver decorated three-dimensional porous architected reduced graphene oxide in polybenzoxazine composites. *New J. Chem.* **2021**, *45*, 16939−16948.
(49) Shayesteh Zeraati, A.; Mende Anjaneyalu, A.; Pawar, S. P.; Abouelmagd, A.; Sundararaj, U. Effect of secondary filler properties and geometry on the electrical, dielectric, and electromagnetic interference shielding properties of carbon nanotubes/polyvinylidene fluoride nanocomposites. *Polym. Eng. Sci.* **2020**, *61*, 959−970.
(50) Li, J.; Qi, S.; Zhang, M.; Wang, Z. Thermal conductivity and electromagnetic shielding effectiveness of composites based on Ag-plating carbon fiber and epoxy. *J. Appl. Polym. Sci.* **2015**, *132*, 42306.
(51) Lee, T.-W.; Lee, S.-E.; Jeong, Y. G. Highly Effective Electromagnetic Interference Shielding Materials based on Silver Nanowire/Cellulose Papers. *ACS Appl. Mater. Interfaces* **2016**, *8*, 13123−13132.
(52) Li, S.; Qian, K.; Thaiboonrod, S.; Wu, H.; Cao, S.; Miao, M.; Shi, L.; Feng, X. Flexible multilayered aramid nanofiber/silver nanowire films with outstanding thermal durability for electromagnetic interference shielding. *Composites, Part A* **2021**, *151*, 106643.
(53) Wang, Y.; Gu, F.-q.; Ni, L.-j.; Liang, K.; Marcus, K.; Liu, S.-l.; Yang, F.; Chen, J.-j.; Feng, Z.-s. Easily fabricated and lightweight PPy/

https://doi.org/10.1021/acsanm.2c00315
ACS Appl. Nano Mater. 2022, 5, 5292−5301

PDA/AgNW composites for excellent electromagnetic interference shielding. *Nanoscale* **2017**, *9*, 18318−18325.

https://doi.org/10.1021/acsanm.2c00315
ACS Appl. Nano Mater. 2022, 5, 5292−5301